LETTERS
PUBLISHED ONLINE: 24 JULY 2011 | DOI: 10.1038/NNANO.2011.118
nature nanotechnology

Deconfinement leads to changes in the nanoscale plasticity of silicon

Dariusz Chrobak[1,2†], Natalia Tymiak[1], Aaron Beaber[3], Ozan Ugurlu[3], William W. Gerberich[3] and Roman Nowak[1,4†*]

Silicon crystals have an important role in the electronics industry, and silicon nanoparticles have applications in areas such as nanoelectromechanical systems, photonics and biotechnology[1,2]. However, the elastic–plastic transition observed in silicon is not fully understood; in particular, it is not known if the plasticity of silicon is determined by dislocations or by transformations between phases. Here, based on compression experiments and molecular dynamics simulations, we show that the mechanical properties of bulk silicon[3–6] and silicon nanoparticles are significantly different. We find that bulk silicon exists in a state of relative constraint, with its plasticity dominated by phase transformations, whereas silicon nanoparticles are less constrained and display dislocation-driven plasticity. This transition, which we call deconfinement, can also explain the absence of phase transformations in deformed silicon nanowedges[7,8]. Furthermore, the phenomenon is in agreement with effects observed in shape-memory alloy nanopillars[9], and provides insight into the origin of incipient plasticity[10–19].

Extensive work has been carried out on the nanodeformation of bulk silicon crystal[3–6]. To determine the mechanical response of silicon nanoparticles, we carried out compression experiments on nanoparticles with radii R in the range 19–169 nm produced by the hypersonic plasma particle deposition technique (see Methods). Load–displacement curves (P–δ) demonstrated two types of behaviour: nanospheres with $R > 57$ nm displayed a characteristic pop-in (PI) event during loading and a push-out (PO) event during unloading, whereas nanospheres with $R < 57$ nm displayed a PI event during loading but no PO event during unloading (Fig. 1a and Supplementary Information). Bulk silicon displays PO behaviour[3–6] (Fig. 1a). When the values of the PO stress and the PI stress are plotted for the nanospheres and bulk silicon (Fig. 1b), the resulting graph strongly suggests that a single process (deconfinement from a bulk state) bridges both phenomena.

The PO singularity of the PI–PO pattern (Fig. 1a and Supplementary Fig. S1a) reflects the pop-out or elbow observed for bulk silicon and constitutes a signature of the onset of the transformation from a β-tin structure (Si-II) to a mixture of Si-XII/III and amorphous (α-Si) phases[3–6]. PO could therefore point to the existence of Si-II in either a stressed bulk crystal (Fig. 1a) or a nanoparticle (Supplementary Fig. S1a), whereas the PI phenomenon (Fig. 1, Supplementary Fig. S1a,b) is unique to silicon nanoparticles. Furthermore, the suppression of Si-II $\rightarrow$ Si-XII/III + α-Si transformation in nanospheres (Fig. 1, Supplementary Fig. S1b) resembles the newly discovered inhibition of a reverse martensitic transformation in shape-memory Cu–Al–Ni nanopillars[9].

Previous electron microscope observations of stressed silicon nanoparticles were unable to detect unequivocally the underlying processes[15,16], so we applied molecular dynamics (MD) simulations to analyse the atomistic mechanisms responsible for nanoscale deformation. MD simulations could not be carried out within our laboratory tests timescale because of the need to resolve atomic-level displacements[20]. The deformation of silicon nanoparticles was therefore approximated by a sequence of transitions between equilibrium states, which made it possible to follow the structural changes in the deformed silicon nanovolume given the absence of thermally activated processes (see Supplementary Information).

The response of stressed silicon nanospheres determined with the Tersoff potential has previously failed to confirm the existence of the PI, PI–PO and PO singularities[18] observed experimentally (Fig. 1), so we modelled silicon crystal using the Stillinger–Weber (SW) potential[21], which accurately reflects both the elastic behaviour and the generation of lattice defects[22]. Compared to the Tersoff[23] and environment-dependent[24] potentials, the SW potential provides the closest match to *ab initio* dislocation nucleation results[22] in defect-free silicon. The deformation history of a silicon nanosphere compressed between two rigid plates (Fig. 2a) has been expressed as a contact pressure versus strain (p_c–ε) relationship derived from MD simulations (see Methods). The initial elastic behaviour of silicon nanoparticles (Fig. 2b) is in accordance with the prediction of classic continuum mechanics expressed by the Hertzian equation[25], which lends support to our approach.

Young's moduli (Fig. 2b) calculated for the nanoparticles ($E_{R1} =$ 122.5 GPa and $E_{R2} = 138.6$ GPa) are lower than those for bulk silicon (160 GPa)[18], and are comparable with the results obtained by Mo *et al.*[26] and Li *et al.*[27]. On the other hand, the confirmed scaling of Young's modulus in tandem with the particle size accounts for the inverse relationship between PI and PO stress (Fig. 1; see Supplementary Information). Maximum contact pressures of 21.3 and 23.5 GPa (Fig. 2b) match the experimentally observed elevated PI stress of silicon nanoparticles (Fig. 1b). Notably, these values are approximately twice as high as those for the hardness of bulk silicon (12 GPa). Moreover, the sudden pressure drop revealed by our simulations (Fig. 2b) is equivalent to the PI observed during the nanoindentation experiments and is attributable to the onset of plasticity in defect-free crystals[10–14,17,19]. Correspondence between the experimental PI stress (~25 GPa) for the smallest nanosphere ($R = 19$ nm, Fig. 1b) and the MD-modelled PI contact pressure (Fig. 2b) is further proof of the validity of our MD procedure with the SW potential.

A deeper insight into the peculiar response of silicon nanospheres (Fig. 1) can be derived from slip vector identification[28] of

[1]Nordic Hysitron Laboratory, School of Chemical Technology, Aalto University, Vuorimiehentie 2A, Espoo, 00076 Aalto, Finland, [2]Institute of Materials Science, University of Silesia, Bankowa 12, 40-007 Katowice, Poland, [3]Department of Chemical Engineering & Materials Science, University of Minnesota, Minneapolis, Minnesota 55455, USA, [4]Extreme Energy-Density Research Institute, Nagaoka University of Technology, Nagaoka, Niigata, 940-2188 Japan; †These authors contributed equally to this work. *e-mail: rnowak@cc.hut.fi

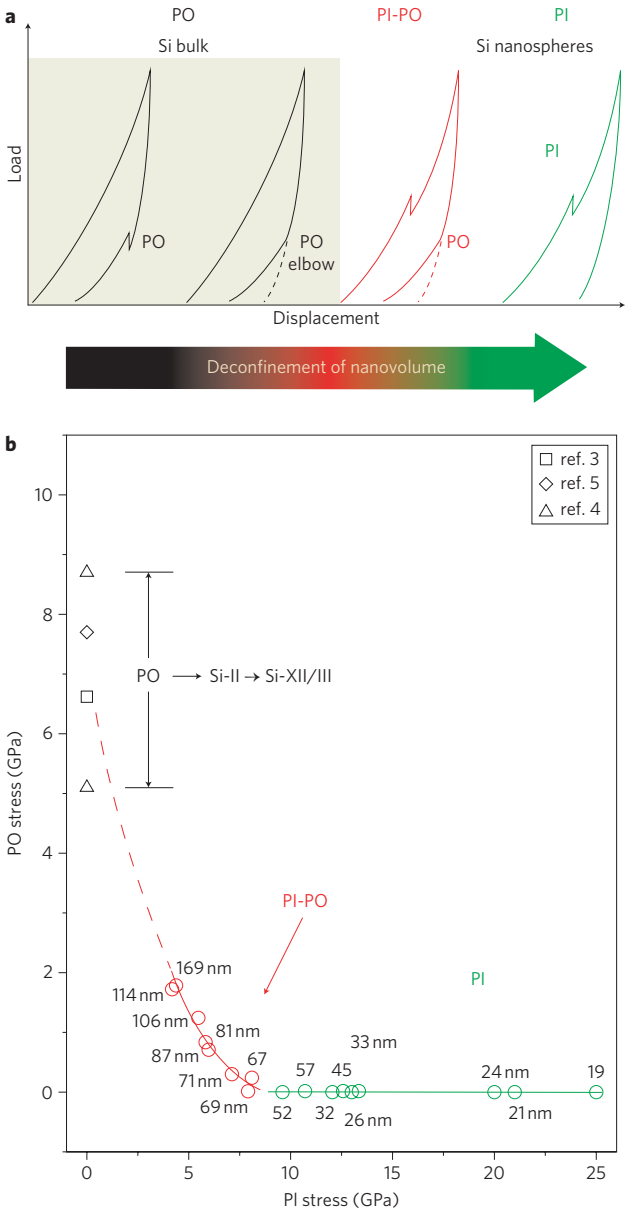

Figure 1 | Mechanical response of nanodeformed silicon from bulk to nanoparticles. a, *P*–δ response of silicon deduced from nanoindentation in bulk[3–6] and our nanocompression experiments on silicon nanospheres (Supplementary Fig. S1). A combination of PI during loading and PO during unloading is denoted the PI–PO effect. The sequence PO → PI–PO → PI indicates a transition from bulk to nanoparticle behaviour. **b**, Results of nanocompression tests on silicon nanospheres with radii of 19–169 nm and bulk silicon nanoindentation data[3–5]. The PI-only (green) response is relevant to the smaller nanospheres ($R \leq 57$ nm), and the PO-only (black) record is characteristic of bulk silicon ($R \rightarrow \infty$). Larger nanoparticles ($R \geq 67$ nm) demonstrate the PI–PO effect (red), covering the transition area between bulk and pure PI response. As PO marks the Si-II → Si-XII/III + α-Si phase transition, its gradual disappearance (PO → PI–PO → PI) with decreasing radius is in accordance with suppression of the reverse martensitic transformation reported for shape-memory alloy nanopillars[9].

the lattice defects. Our results demonstrate that, at the PI stage, a set of perfect dislocations (Burgers vector length of 3.84 Å) is created inside the silicon nanosphere with a radius of 10 nm (Fig. 2c and animations in Supplementary Information). Even at the initial stage of unloading, one of the dislocation loops reaches the surface and creates a permanent step, thereby producing a tiny

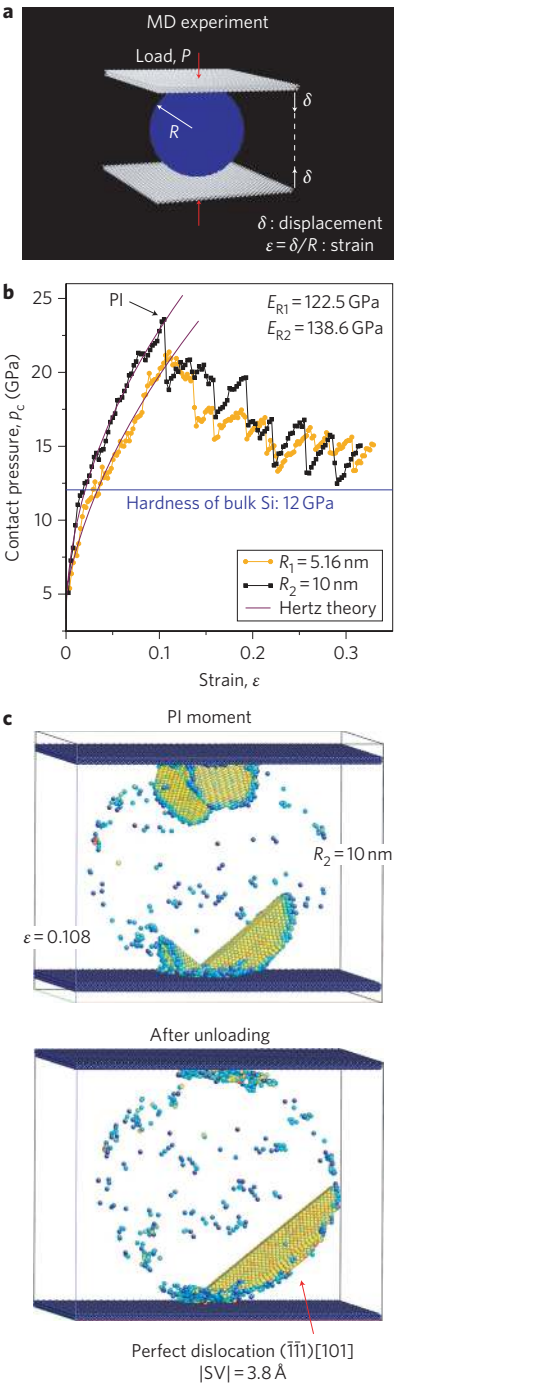

Figure 2 | Mechanical response of a compressed silicon nanoparticle. **a**, MD simulations of silicon nanospheres compressed between two rigid plates. Displacement δ under applied load P is quantified in terms of $\varepsilon = \delta/R$ strain. **b**, Contact pressure ($p_c = P/A$, where A is contact area) versus strain relationship (p_c–ε) demonstrates that the maximum value of p_c reached in the nanoparticles (21.3–23.5 GPa) is nearly double that (~12 GPa) of bulk silicon[18]. Elastic deformation follows Hertzian theory[25] (solid line). After the PI (onset of plasticity), multiple singularities reflect the nature of plasticity. **c**, Slip vector (SV) analysis of the unstable dislocation structure of the silicon nanoparticle ($R_2 = 10$ nm). Perfect dislocation loops ($|SV| = 3.8$ Å, $b = |1/2[101]| = 3.84$ Å, atoms marked in yellow) nucleate immediately after the PI ($\varepsilon = 0.108$), and terminate inside the nanosphere. After unloading, a majority of the dislocation loops vanish, whereas those at the nanoparticle surface stabilize, hence the nearly complete silicon particle shape recovery following a PI, referred to as 'reversible plasticity'[15].

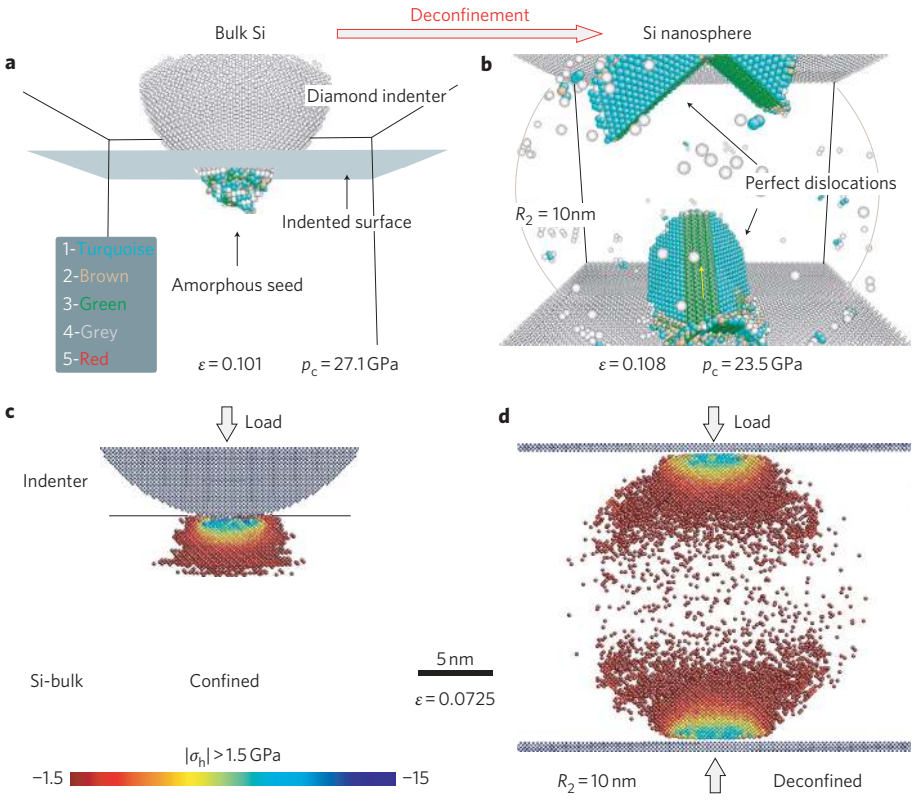

Figure 3 | MD-simulated contrasting behaviour of confined (bulk) and deconfined (nanoparticle) silicon. a, Initial plastic deformation of bulk silicon indented with a diamond sphere ($R = 10$ nm). As strain reaches $\varepsilon = 0.101$, the deformed volume under the indentation contact displays no evidence of dislocations. Coordination numbers ranging from 1 to 5 suggest an amorphous structure. **b**, Plasticity initiation in a compressed silicon nanosphere. Despite similar levels of strain, the mechanisms of plasticity in the silicon nanoparticle and bulk are essentially different. Plastic deformation in a nanoparticle begins with perfect dislocation loops (atoms marked in turquoise) joined by stacking fault regions (atoms marked in green). Perfect dislocations to the left and right of the yellow arrow lie on the $(\bar{1}11)$ and $(11\bar{1})$ planes, respectively, whereas the stacking fault joining them is positioned on the $(10\bar{1})$ plane. **c**,**d**, Distribution of hydrostatic pressure (σ_h) in bulk silicon (**c**) and in the silicon nanosphere ($R = 10$ nm, **d**), both strained elastically up to $\varepsilon = 0.0725$. Atoms exposed to pressures higher than $|\sigma_h| \geq 1.5$ GPa are marked in colours, indicating a higher stress concentration in confined silicon (**c**) than in the nanoparticle (**d**). Note that both distributions are presented on a common scale.

irreversible deformation (Supplementary Fig. S2). The remaining dislocation loops contract and disappear, accounting for the partially reversible plastic behaviour confirmed by previous experiments[15,16], and vindicating the results of our simulations. The slip vector also uncovered differences in the structure stability of two silicon nanoparticles ($R_1 = 5.16$ nm, $R_2 = 10$ nm) within the group that exhibited a PI response (Fig. 1). The onset of plasticity in the smaller of the two nanospheres therefore involved the creation of a stacking fault, in contrast to the behaviour of the larger nanosphere described above (for details see Supplementary Information).

Silicon nanospheres are therefore behaving like a material of a different order, namely, with dislocation activity playing a crucial role in their mechanical response (Fig. 2c). This contrasts with the commonly recognized dominance of phase transformation in the plastic deformation of bulk silicon[3–6]. It also contrasts with the phase-transition-type deformation discovered for nanoscale GaAs crystal[17,19]. Why, therefore, should the phase transformation (which resembles the suppression of the martensitic transformation in CuAlNi nanopillars[9]) fail to occur during the testing of silicon nanospheres with radii below 57 nm (Fig. 1b)?

From our results (Figs 1 and 2, and Supplementary Figs S1 and S2), we can suggest that the observations do not stem exclusively from the size of the deformed volume (size effect) but from the fact that it terminates on the free surface; that is, the nanovolume in question is less constrained, being deconfined from the bulk state. The behaviour cannot be the result of the well-known size effect[8,29], because the nanovolume deformation induced during indentation of bulk silicon does not produce the PI and PI–PO event.

MD simulations involving bulk silicon (see Methods) probed with a spherical indenter (radius, 10 nm) confirmed that a dislocation-driven onset of plasticity is unique to silicon nanoparticles

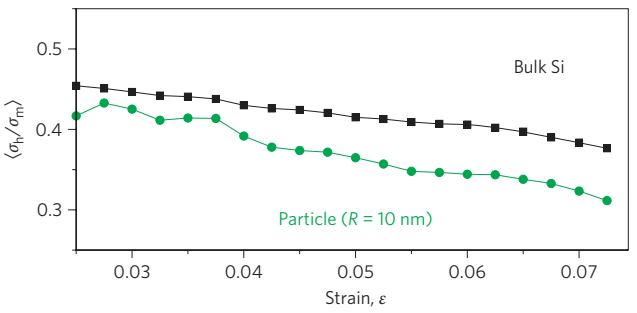

Figure 4 | Effect of deconfinement of silicon from bulk to nanosphere viewed in terms of stress analysis. Averaged ratio of hydrostatic (σ_h) and von Mises stresses (σ_m) determined using MD calculations during consecutive steps of elastic deformation. The $\langle\sigma_h/\sigma_m\rangle$ values calculated for the nanoparticle (green) are systematically lower than those obtained for the bulk state (black), which suggests that the silicon particle is prone to undergo non-dilatational strain rather than the volumetric strain dominant in bulk.

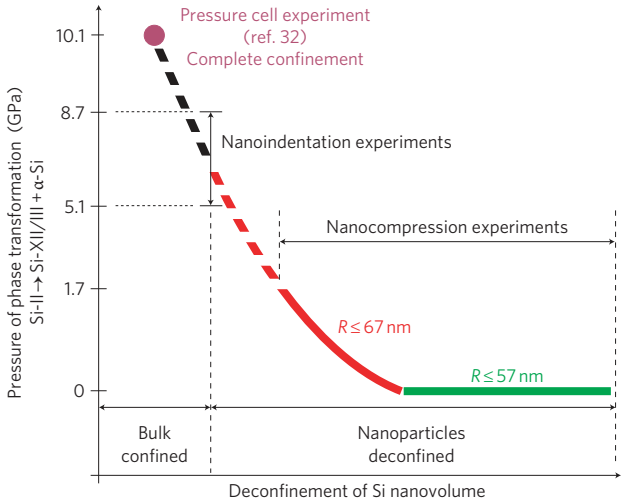

Figure 5 | Schematic of silicon deconfinement process scaled with the pressure of the Si-II → Si-XII/III + α-Si phase transition. General relationship determined by means of nanocompression experiments (green and red solid lines) for highly deconfined silicon (nanoparticles) appears to extrapolate for larger nanoparticles (red broken line) towards the data obtained for bulk silicon deformed by nanoindentation (black area). When the entire free surface of the bulk is under external high pressure, it is possible to imagine such a material as being 'confined to a higher degree' (with virtually no free surface). This is exactly what happens to silicon deformed in pressure cell experiments[33], in which the characteristic pressure of the Si-II → Si-XII/III transformation (magenta point) is certainly higher than for the nanoindented bulk crystal (black area). Note that in the deconfined state, silicon deforms with the contribution of phase transformation, but for higher degrees of deconfinement, there is no transformation at all (green solid line). The schematic thus constitutes a roadmap for a range of materials deconfined from their bulk state to nanoparticle, nanowire, nanowedge or nanopillar (cf. ref. 9).

(Fig. 3). The plasticity of the bulk silicon starts from the inception of an amorphous zone with coordination numbers of the atoms ranging from 1 to 5 (Fig. 3a), which complies with previous observations[30]. The notable difference between the mechanism of plastic deformation in the nanoindented bulk silicon crystal (Fig. 3a) and that of the compressed nanospheres (Fig. 3b) demonstrates that it is difficult to predict the deformation of nanoparticles from the characterization of bulk surfaces.

Additional insight on the deconfinement effect (see Methods) is provided by observing the discrepancy in the distribution of hydrostatic pressure generated during an elastic nanodeformation of bulk silicon on the one hand and the compression of nanoparticles on the other (cf. Figs 3c and d). In contrast to the highly stressed fraction of bulk silicon restricted to a tiny volume directly under the tip, the stress in the silicon nanoparticle is spread considerably wider, involving atoms from virtually the entire particle volume (Fig. 3d). This happens despite both bulk and nanosphere being strained to the same degree ($\varepsilon = 0.0725$).

Neither the hydrostatic pressure responsible for volumetric changes nor the von Mises stress accountable for shape evolution are able, individually, to explain the nature of the observed property alteration (Figs 1 and 2). Our solution to the problem is to use an averaged ratio of hydrostatic (σ_h) and von Mises (σ_m) stresses (Fig. 4), which has proved capable of detecting the dominant deformation mode for semiconductors[31]. The $\langle\sigma_h/\sigma_m\rangle$ values calculated for atoms subjected to hydrostatic pressure in excess of 1.5 GPa (Fig. 3c,d) are systematically lower for nanoparticles than the bulk state. This suggests that silicon nanoparticles tend to deform with a limited contribution of the volumetric strain that dominates the bulk response. Further stages of loading result in phase transformation at the onset of plasticity in nanodeformed bulk silicon, while the increasing role of shearing stress in nanoparticles leads to dislocation-controlled plastic deformation. Unexpectedly, this result is independent of the orientation (as is evident in Supplementary Fig. S7), and corresponds with our experimental data (Fig. 1).

All the above lead us to propose the concept of deconfinement to reflect a transition from bulk to nanoparticle behaviour, a process in which deformation is driven by a distinctive set of mechanisms (Figs 1, 3 and 4), resulting in an alteration of the properties of silicon. It is therefore deconfinement that leads to a shift from phase-transformation-dominated incipient plasticity to a dislocation-driven one, exemplified by the PO → PI–PO → PI sequence (Fig. 1).

Figure 5 illustrates the generality of the concept, which ranges from cell pressure experiments[32] through nanoindentation of bulk silicon[3–6] to compressed silicon nanoparticles. Independent support for the concept is provided by work on both Cu–Al–Ni alloy nanopillars[9] and silicon nanowedges[7–9]. Conversely, the results of our compression experiments (Fig. 1) and atomistic simulations (Figs 2 to 4, Supplementary Fig. S2) have implications for the work of Minor *et al.*[7] and Ge *et al.*[8], whose findings can now be re-interpreted as an idiosyncrasy of the deconfinement phenomenon. Our results were obtained for smooth-surface nanospheres and thus suggest that no surface singularity is necessary to obtain dislocation-governed plasticity in silicon.

Methods

Fabrication of silicon nanoparticles and nanomechanical experiments. The hypersonic plasma particle deposition (HPPD) technique[33] used for synthesis of silicon nanoparticles makes use of an argon–hydrogen plasma containing injected vapour-phase silicon tetrachloride. Silicon nanoparticles were placed on a sapphire substrate and squeezed in a transmission electron microscope-based indentation tester. The instrument was equipped with a large-radius diamond tip for compressing the evaluated nanosphere. The idea of the experiment was to squeeze the nanospheres between parallel and rigid surfaces. With the help of recorded load–displacement data, the contact stresses on the investigated nanoparticle were determined. Contact strains were estimated using the Tabor approximation (for details see Supplementary Information).

Molecular dynamics simulations. MD computations were performed using the LAMMPS simulation code (http://lammps.sandia.gov/) for two sizes of silicon nanospheres ($R_1 = 5.16$ nm, 30,691 atoms and $R_2 = 10$ nm, 219,277 atoms), compressed between horizontal plates along the [001] silicon direction and, additionally, for a block of bulk silicon ($27.16 \times 27.16 \times 22.81$ nm^3, 615,000 atoms) indented with a spherical diamond tip ($R = 10$ nm) in the (001) plane. Interactions among the silicon atoms within the diamond structure were described using the SW potential[21]. The atomic structure of the deformed silicon volumes was relaxed in 20,000 time steps (in total, 40 ps) for each displacement increment at a temperature of 300 K. The symmetrical displacement increments of $\delta_1 = 0.1$ Å and $\delta_2 = 0.25$ Å were repeatedly applied to both plates (Fig. 2a), to accomplish the loading path for the smaller and bigger silicon nanosphere, respectively. This produced strain increments of $\Delta\varepsilon_1 = 0.0020$ and $\Delta\varepsilon_2 = 0.0025$. Interactions between the diamond and silicon (indenter tip–bulk silicon crystal; rigid plates–silicon nanosphere) were modelled with the repulsive term of the Lennard–Jones potential (cutoff radius, 4 Å). The loading of silicon was characterized by the mean contact pressure $p_c = P/A$, where the contact area A was estimated by determining the number of silicon atoms experiencing a non-zero interaction with the contacting surface. The defect structure was visualized using slip-vector analysis[28], with a slip threshold value of 1 Å. Hydrostatic (σ_h) as well as von Mises (σ_m) stresses generated in the nanoindented bulk silicon and compressed silicon nanosphere ($R = 10$ nm) were determined for the [001], [110] and [111] orientations of the loading axis. The $\langle\sigma_h/\sigma_m\rangle$ ratio in particular proved capable of detecting the alteration in the nanodeformation mechanism.

Received 4 January 2011; accepted 17 June 2011;
published online 24 July 2011

References

1. Ting, Z. & Li, J. Ultra-strength materials. *Progr. Mater. Sci.* **55,** 710–757 (2010).
2. Craighead, H. G. Nanoelectromechanical systems. *Science* **290,** 1532–1535 (2000).

3. Domnich, V., Gogotsi, Y. & Dub, S. Effect of phase transformations on the shape of the unloading curve in the nanoindentation of silicon. *Appl. Phys. Lett.* **76,** 2214–2216 (2000).
4. Juliano, T., Domnich, V. & Gogotsi, Y. Examining pressure-induced phase transformations in silicon by spherical indentation and Raman spectroscopy: a statistical study. *J. Mater. Res.* **19,** 3099–3108 (2004).
5. Chang, L. & Zhang, L. C. Deformation mechanisms at pop-out in monocrystalline silicon under nanoindentation. *Acta Mater.* **57,** 2148–2153 (2009).
6. Bradby, J. E., Williams, J. S. & Swain, M. V. *In situ* electrical characterization of phase transformations in Si during indentation. *Phys. Rev. B* **67,** 085205 (2003).
7. Minor, A. M. *et al*. Room temperature dislocation plasticity in silicon. *Phil. Mag.* **85,** 323–330 (2005).
8. Ge, D., Minor, A. M., Stach, E. A. & Morris, J. W. Size effects in the nanoindentation of silicon at ambient temperature. *Phil. Mag.* **86,** 4069–4080 (2006).
9. San Juan, J., No, M. L. & Schuh, C. A. Nanoscale shape-memory alloys for ultrahigh mechanical damping. *Nature Nanotech.* **4,** 415–419 (2009).
10. Li, J., Van Vliet, K. J., Zhu, T., Yip, S. & Suresh, S. Atomistic mechanisms governing elastic limit and incipient plasticity in crystals. *Nature* **418,** 307–310 (2002).
11. Szlufarska, I. Nakano, A. & Vashishta, P. A Crossover in the mechanical response of nanocrystalline ceramics. *Science* **309,** 911–914 (2005).
12. Schuh, C. A. Mason, J. K. & Lund, A. C. Quantitative insight into dislocation nucleation from high-temperature nanoindentation experiments. *Nature Mater.* **4,** 617–621 (2005).
13. Mason, J. K., Lund, A. C. & Schuh, C. A. Determining the activation energy and volume for the onset of plasticity during nanoindentation. *Phys. Rev. B* **73,** 054102 (2006).
14. Gerberich, W. W. & Mook, W. M. Nanomechanics: a new picture of plasticity. *Nature Mater.* **4,** 577–578 (2005).
15. Gerberich, W. W. *et al*. Superhard silicon nanospheres. *J. Mech. Phys. Solids* **51,** 979–992 (2003).
16. Gerberich, W. W. *et al*. Reverse plasticity in single crystal silicon nanospheres. *Int. J. Plast.* **21,** 2391–2405 (2005).
17. Chrobak, D., Nordlund, K. & Nowak, R. Nondislocation origin of GaAs nanoindentation pop-in event. *Phys. Rev. Lett.* **98,** 045502 (2007).
18. Valentini, P., Gerberich, W. W. & Dumitrica, T. Phase-transition plasticity response in uniaxially compressed silicon nanospheres. *Phys. Rev. Lett.* **99,** 175701 (2007).
19. Nowak, R. *et al*. An electric current spike linked to nanoscale plasticity. *Nature Nanotech.* **4,** 287–291 (2009).
20. Nowak, R., Yoshida, F., Chrobak, D., Kurzydlowski, K. J., Takagi T. & Sasaki, T. in *Encyclopedia of Nanoscience and Nanotechnology* (ed. Nalwa, S. H.) 313–374 (American Scientific, 2010).
21. Stillinger, F. H. & Weber, T. A. Computer simulation of local order in condensed phases of silicon. *Phys. Rev. B* **31,** 5262–5271 (1985).
22. Godet, J., Pizzagalli, L., Brochard, S. & Beauchamp, P. Theoretical study of dislocation nucleation from simple surface defects in semiconductors. *Phys. Rev. B* **70,** 054109 (2004).
23. Tersoff, J. New empirical approach for the structure and energy of covalent systems. *Phys. Rev. B* **37,** 6991–7000 (1988).
24. Bazant, M. Z., Kaxiras, E. & Justo, J. F. Environment-dependent interatomic potential for bulk silicon. *Phys. Rev. B* **56,** 8542–8552 (1997).
25. Hertz, H. Über die Berührung fester elastischer Körper. *J. Reine Angew. Math.* **92,** 156–171 (1882).
26. Mo, Y., Turner, K. T. & Szlufarska, I. Friction laws at the nanoscale. *Nature* **457,** 1116–1119 (2009).
27. Li, X., Ono, T. & Wang, Y. & Esashi, M. Ultrathin single crystalline silicon cantilever resonators: fabrication technology and significant specimen size effect on Young's modulus, *Appl. Phys. Lett.* **83,** 3081–3083 (2003).
28. Zimmerman, J. A., Kelchner, C. L., Klein, P. A., Hamilton, J. C. & Foiles, S. M. Surface step effects on nanoindentation. *Phys. Rev. Lett.* **87,** 165507 (2001).
29. Choi, Y., Van Vliet, K. J., Li, J. & Suresh, S. Size effects on the onset of plastic deformation during nanoindentation of thin films and patterned lines. *J. Appl. Phys.* **94,** 6050–6058 (2003).
30. Wu, Y. Q. & Xu, Y. B. Lattice-distortion-induced amorphization in indented [110] silicon. *J. Mater. Res.* **14,** 682–687 (1999).
31. Lorenz, D. *et al*. Pop-in effect as homogeneous nucleation of dislocations during nanoindentation. *Phys. Rev. B* **67,** 172101 (2003).
32. Piltz, R. O. *et al*. Structure and properties of silicon XII: a complex tetrahedrally bonded phase. *Phys. Rev. B* **52,** 4072–4085 (1995).
33. Rao, N. P. *et al*. Hypersonic plasma particle deposition of nanostructured silicon and silicon carbide. *J. Aerosol Sci.* **29,** 707–720 (1998).

Acknowledgements

The authors gratefully acknowledge the CSC–IT Center for Science for computation resources and the Ceramic Society of Japan for invaluable assistance. R.N., D.C. and N.T. thank the Academy of Finland for partial support under the FINNANO programme and NANOSPIKE research project. A.B. and W.W.G. acknowledge the support of the National Science Foundation (NSF; CTS-0506748 and CMMI-00800896). R.N. acknowledges the involvement of the Research Foundation of Helsinki University of Technology, as well as the NANOINDENT EU-research grant. D.C. and R.N. thank R. Nieminen and K. Niihara for valuable discussions. The authors also thank A. Poludniak for careful reading of the manuscript and stimulating comments.

Author contributions

D.C. carried out the calculations and analysed the compatibility of the theoretical and experimental data. R.N. conceived the concept of deconfinement-driven transition and designed the research project. N.T. analysed the data. W.W.G. designed and supervised the experimental part, and A.B. and O.U. performed nanocompression tests and analysed the output. R.N. and D.C. wrote the paper. All authors discussed the results.

Additional information

The authors declare no competing financial interests. Supplementary information accompanies this paper at www.nature.com/naturenanotechnology. Reprints and permission information is available online at http://www.nature.com/reprints. Correspondence and requests for materials should be addressed to R.N.